Analysis of Vickers Hardness by the Finite Element Method

Y. Murakami
Department of Mechanical Science and Engineering, Faculty of Engineering, Kyushu University, Hakozaki, Fukuoka 812, Japan
Mem. ASME

K. Matsuda
Department of Mechanical Engineering, Kyushu Institute of Technology, Kitakyushu 804, Japan

A particular formulation of the three-dimensional finite element method specifically for analyzing the Vickers hardness test is established. The Vickers hardness of 0.46 percent carbon steel and 70/30 brass is calculated using the proposed method using the stress-strain curve obtained from a tensile test. The calculated values correlate well with the experimental results for 0.46 percent steel and 70/30 brass. In addition, the analysis predicts the extension of the plastic zone induced by indentation, the stresses at the maximum load, and the residual stresses present after complete removal of the load. At the maximum load there are no tensile stresses in the vicinity of the indenter. However, after removal of the load, large tensile residual stresses are present on the diagonal edge beneath the indentation in the direction perpendicular to the diagonal edge. These results imply that it is necessary to reconsider the accuracy and validity of the conventional indentation method used for the determination of K_{Ic} *for brittle materials such as ceramics.*

1 Introduction

For many years, Vickers hardness testing of ductile materials has been used to measure hardness, one of the basic mechanical properties. Recently, the Vickers hardness testing technique has been considered as a possible method for the determination of additional material properties in brittle materials such as the fracture toughness, K_{Ic}. In addition, it may also be used to evaluate the strength of thin coatings and the measurement of near surface residual stresses.

However, to date there are 19 published formulae (Ponton and Rowlings, 1989)) relating the measured micro-indentation-induced crack length with K_{Ic}. This abundance of different formulae is due to the fact that the Vickers hardness test has never been completely analyzed. Such an analysis forms the subject of this paper.

The correlation of the Vickers hardness with other mechanical properties has been studied mostly by experiment only (Tabor, 1951; Yoshizawa, 1967; Westbrook and Conrod, 1973). There have been a few theoretical and analytical studies (Perrott, 1977; Chiang, Marshall, and Evans, 1982; Tanaka, 1984; Yoshino and Yamada, 1984; Mura, Yamashita, Mishima, and Hirose, 1989), however, these do not appear to satisfy the exact boundary conditions and their accuracy is insufficient for analysis of the Vickers hardness test Hv for engineering materials.

An accurate numerical analysis is necessary for a systematic investigation of the effects of the mechanical properties on Hv and thus gain a thorough understanding of the related phenomena.

Although the development of the finite element method has progressed over the years, indentation problems such as the Vickers hardness test cannot be solved using conventional commercial finite element method software as commercial programs are unable to simulate interface contact problems to the accuracy required for this particular purpose. For this reason the finite element method solutions for the Vickers hardness test have yet to be published despite many demands from experimental researchers.

In this paper, a particular formulation for indenting the specimen with a diamond pyramid is established. An accurate analysis of the Vickers hardness requires a special formulation of the three-dimensional finite element method based on the strain incremental plastic theory (Prandtl-Reuss equation (Zienkiewicz, 1971)). The Vickers hardness of 0.46 percent carbon steel and 70/30 brass is analyzed by the proposed method.

To confirm the validity of the proposed method, numerical values for indentation diagonal size and hardness are compared with experimental results. Finally, after investigating the stress distribution in the vicinity of the indentation at the maximum load and after unloading, the validity of the conventional indentation method for measuring the fracture toughness K_{Ic} for materials such as ceramics is discussed.

2 Finite Element Formulation for the Vickers Hardness Analysis

2.1 Displacement Boundary Conditions. The Vickers hardness Hv is defined as the load divided by the surface area of a square diamond pyramid indentation with top angle of 136 degrees. Since it is expected that the diamond indenter barely deforms during the hardness test, we regard the indenter as a rigid body.

Contributed by the Applied Mechanics Division of THE AMERICAN SOCIETY OF MECHANICAL ENGINEERS for publication in the ASME JOURNAL OF APPLIED MECHANICS.
Discussion on this paper should be addressed to the Technical Editor, Professor Lewis T. Wheeler, Department of Mechanical Engineering, University of Houston, Houston, TX 77204-4792, and will be accepted until four months after final publication of the paper itself in the ASME JOURNAL OF APPLIED MECHANICS.
Manuscript received by the ASME Applied Mechanics Division, Oct. 30, 1992; final revision, May 22, 1993. Associate Technical Editor: W. N. Sharpe, Jr.

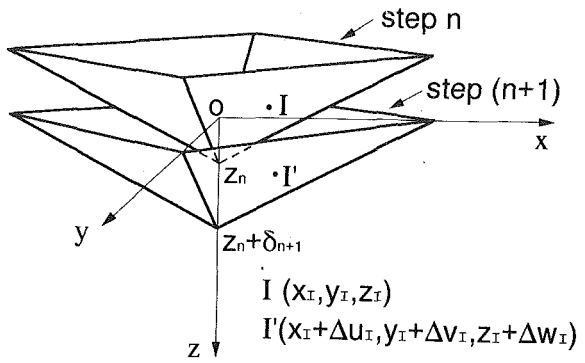

Fig. 1 Displacement boundary condition

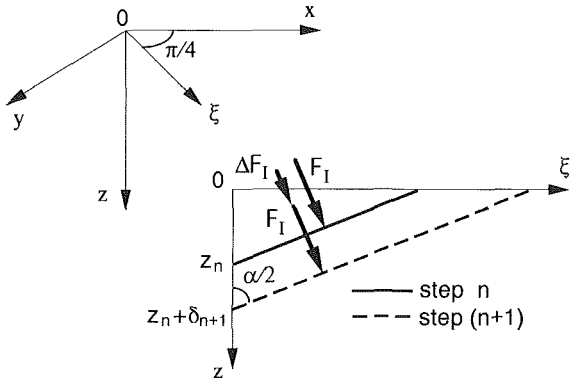

Fig. 2 Load boundary condition

Figure 1 shows the beginning of step n of the indentation process. The equation of the indenter surface can be written as

$$C_x x + C_y y + C_z(z - z_n) = 0 \quad (x \geq 0,\ y \geq 0). \tag{1}$$

At the beginning of step $(n+1)$, the equation of the indenter surface is given by

$$C_x x' + C_y y' + C_z(z' - z_n - \delta_{n+1}) = 0 \tag{2}$$

where δ_{n+1} is the incremental displacement of the indenter in the z-direction in step $n+1$, and C_x, C_y and C_z are the direction cosines of the indenter surface defined by

$$C_x = C_y = \cos(\alpha/2)/\sqrt{2}$$
$$C_z = \sin(\alpha/2). \tag{3}$$

In Fig. 1, I and I' indicate a nodal point on the contact surface of the specimen at steps n and $(n+1)$, respectively. (x_I, y_I, z_I) are the coordinates and $(\Delta u_I, \Delta v_I, \Delta w_I)$ are the incremental displacements of node I. Substituting the coordinates I' $(x_I+\Delta u_I, y_I+\Delta v_I, z_I+\Delta w_I)$ into Eq. (2), gives

$$C_x(x_I+\Delta u_I) + C_y(y_I+\Delta v_I) + C_z(z_I+\Delta w_I - z_n - \delta_{n+1}) = 0. \tag{4}$$

From Eq. (1), the following is obtained:

$$C_x\Delta u_I + C_y\Delta v_I + C_z(\Delta w_I - \delta_{n+1}) = 0. \tag{5}$$

Using Eq. (3),

$$\Delta u_I + \Delta v_I + \beta(\Delta w_I - \delta_{n+1}) = 0$$
$$[\beta = C_z/C_x = C_z/C_y = \sqrt{2}\tan(\alpha/2)]. \tag{6}$$

Equation (6) is therefore the displacement boundary condition.

2.2 Load Boundary Condition. In this situation, the contact surface of the hardness specimen is assumed to be frictionless. Therefore, the pressure at the contact surface acts in the normal direction. Denoting the x, y, and z components of the nodal force of node I by F_{Ix}, F_{Iy}, and F_{Iz} (see Fig. 2), we can write the load boundary condition at the contact surface under the condition of no friction as follows:

$$F_{Ix}/C_x = F_{Iy}/C_y = F_{Iz}/C_z (= F_I). \tag{7}$$

Denoting the incremental nodal force of node I in normal direction by ΔF_I, its x, y, and z-components ΔF_{Ix}, ΔF_{Iy}, and ΔF_{Iz} must satisfy the following condition:

$$\Delta F_{Ix}/C_x = \Delta F_{Iy}/C_y = \Delta F_{Iz}/C_z (= \Delta F_I). \tag{8}$$

Substituting Eq. (3) into (8), gives

$$\Delta F_{Ix} = \Delta F_{Iy} = \Delta F_{Iz}/\beta. \tag{9}$$

Equation (9) is therefore the incremental load boundary condition at the contact surface.

2.3 Formulation of Incremental Loading Process. Considering the incremental loads ΔF_{Ix}, ΔF_{Iy}, and ΔF_{Iz}, the simultaneous equations for nodes at the contact surface can be written as follows:

$$\begin{bmatrix} \vdots & \vdots & \vdots \\ \cdots\ k_{3I-2,3I-2} & k_{3I-2,3I-1} & k_{3I-2,3I}\ \cdots \\ \cdots\ k_{3I-1,3I-2} & k_{3I-1,3I-1} & k_{3I-1,3I}\ \cdots \\ \cdots\ k_{3I,3I-2} & k_{3I,3I-1} & k_{3I,3I}\ \cdots \\ \vdots & \vdots & \vdots \end{bmatrix} \begin{Bmatrix} \vdots \\ \Delta u_I \\ \Delta v_I \\ \Delta w_I \\ \vdots \end{Bmatrix} = \begin{Bmatrix} \vdots \\ \Delta F_{Ix} \\ \Delta F_{Iy} \\ \Delta F_{Iz} \\ \vdots \end{Bmatrix} \tag{10}$$

where k's are the finite element method incremental elastic-plastic stiffness matrix components. The equation for the remaining nodes are the same as those which are used in conventional finite element method. From Eq. (9), the line $(3I)$ in Eq. (10) is divided by $-\beta(=-\sqrt{2}\tan(\alpha/2))$ and added to the lines $(3I-2)$ and $(3I-1)$, ΔF_{Ix} and ΔF_{Iy} can then be eliminated from Eq. (10). The following is obtained:

$$\begin{bmatrix} \vdots & \vdots & \vdots & \vdots \\ k_{3I-2,1}-k_{3I,1}/\beta\ \cdots & k_{3I-2,3I-2}-k_{3I,3I-2}/\beta & k_{3I-2,3I-1}-k_{3I,3I-1}/\beta & k_{3I-2,3I}-k_{3I,3I}/\beta\ \cdots \\ k_{3I-1,1}-k_{3I,1}/\beta\ \cdots & k_{3I-1,3I-2}-k_{3I,3I-2}/\beta & k_{3I-1,3I-1}-k_{3I,3I-1}/\beta & k_{3I-1,3I}-k_{3I,3I}/\beta\ \cdots \\ k_{3I,1}\ \cdots & k_{3I,3I-2} & k_{3I,3I-1} & k_{3I,3I}\ \cdots \\ \vdots & \vdots & \vdots & \vdots \end{bmatrix} \begin{Bmatrix} \vdots \\ \Delta u_I \\ \Delta v_I \\ \Delta w_I \\ \vdots \end{Bmatrix} = \begin{Bmatrix} \vdots \\ 0 \\ 0 \\ \Delta F_{Iz} \\ \vdots \end{Bmatrix}. \tag{11}$$

Replacing the line $(3I)$ of Eq. (11) by the displacement boundary condition (6) gives

$$\begin{bmatrix} \vdots & \vdots & \vdots & \vdots \\ k_{3I-2,1}-k_{3I,1}/\beta\ \cdots & k_{3I-2,3I-2}-k_{3I,3I-2}/\beta & k_{3I-2,3I-1}-k_{3I,3I-1}/\beta & k_{3I-2,3I}-k_{3I,3I}/\beta\ \cdots \\ k_{3I-1,1}-k_{3I,1}/\beta\ \cdots & k_{3I-1,3I-2}-k_{3I,3I-2}/\beta & k_{3I-1,3I-1}-k_{3I,3I-1}/\beta & k_{3I-1,3I}-k_{3I,3I}/\beta\ \cdots \\ \cdots 0 \cdots & 1.0 & 1.0 & \beta\ \cdots 0 \cdots \\ \vdots & \vdots & \vdots & \vdots \end{bmatrix} \begin{Bmatrix} \vdots \\ \Delta u_I \\ \Delta v_I \\ \Delta w_I \\ \vdots \end{Bmatrix} = \begin{Bmatrix} \vdots \\ 0 \\ 0 \\ \beta\delta_{n+1} \\ \vdots \end{Bmatrix}. \tag{12}$$

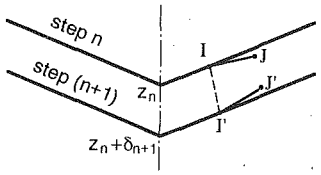

Fig. 3 Correction of the incremental displacement

Thus, Eq. (12) is the final formulation for the analysis of the Vickers hardness, though a sufficiently small incremental displacement δ_n must be given to obtain accurate solutions.

2.4 Particular Numerical Procedure to Satisfy the Conditions of Indenter Contact Surface. Equation (6) is the condition which the nodal displacements at the contact surface must satisfy to maintain the contact surface pyramid. Figure 3 illustrates that node J near the indenter surface at step n enters the indenter domain at step $(n+1)$. In this case

$$x_J+\Delta u_J+y_J+\Delta v_J+\beta(z_J+\Delta w_J-z_n-\delta_{n+1})\geq 0 \qquad (13)$$

is not satisfied. Therefore, a constant m_J is determined which satisfies the following equation:

$$x_J+m_J\Delta u_J+y_J+m_J\Delta v_J+\beta(z_J+m_J\Delta w_J-z_n-m_J\delta_{n+1})=0. \qquad (14)$$

The minimum value of m_J for an arbitrary node is denoted $m_{\min}$ and satisfies the relation $0.0<m_{\min}<1.0$. $m_{\min}\delta_{n+1}$ is thus considered as the modified incremental indenter displacement to ensure that the particular node does not penetrate the specimen surface at the end of the step.

2.5 The Finite Element Method Program. A three-dimensional finite element method based on the strain incremental plastic theory Prandtl-Reuss equation (Zienkiewicz (1971)) is used for the numerical analysis of the Vickers hardness test. Unless otherwise stated, the isotropic hardening rule was used for specifying the dependence of the yield condition on plastic strain and deformation history. The deformation of the specimen is determined by adding incremental displacement to the node coordinates. The number of displacement increments during loading and unloading is 335 for 0.46 percent C steel and 295 for 70/30 brass. Therefore, the calculation for a single increment is sufficiently small to obtain accurate solutions by the small strain incremental plastic theory.

2.6 The Finite Element Method Mesh and Boundary Conditions. Figure 4 shows the finite element method mesh, the design of which is based on the particular characteristics of the Vickers indentation test. An inverted pyramid (Fig. 4(*a*)) was used for the initial shape of the specimen. The x and y-axes coincide with the direction of the diagonals of the base surface of the pyramid. The symmetry of the shape ensures that only the region $x\geq 0$, $y\geq 0$ needs to be analyzed. Tetrahedral elements are generally used to compose the total specimen with 581 nodes and 2376 elements. To avoid using a complicated mesh, units of triangular column elements or rectangular parallelepipeds composed with some tetrahedral elements may be used to build the total pyramid. However, if coarse and fine meshes are mixed, flat elements are inevitably produced.

In this analysis, truncated triangular pyramids with tetrahedral elements are initially created. This base layer is then built up to make and piled them up to the total triangular the whole pyramid as shown in Fig. 4(*d*). The volume of individual elements are initially created. This base layer is then built up to make contained in truncated triangular pyramids from the first to sixth stage remains unchanged. Each truncated triangular pyramid above the seventh stage has an equal numbers of elements: 216. Thus, it is possible to change the size of

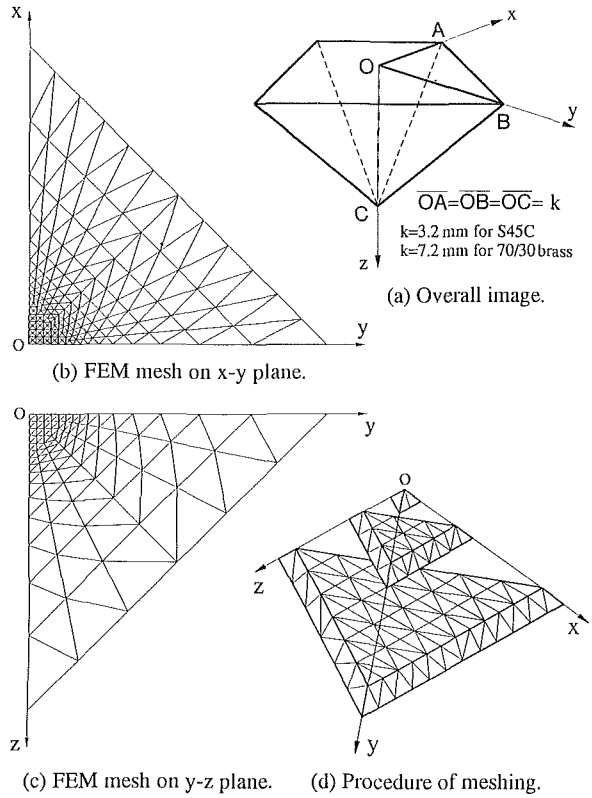

Fig. 4 Finite element mesh

truncated triangular pyramids which have close geometrical similarity. If the nodes are numbered in order from the top stage (the coordinate origin), the bandwidth of the stiffness matrix does not change after seven stages. This reduces computer storage requirements.

The symmetric displacement boundary condition for the y-z plane is $\Delta u=0$ and that for z-x plane is $\Delta v=0$. Considering the results of the preliminary calculations (see Sec. 3.1), the boundary conditions for the side plane of the total pyramid (ABC in Fig. 4(*a*)) were considered to be $\Delta u=\Delta v=\Delta w=0$.

3 Numerical Results and Comparison With Experimental Results

To confirm the validity and accuracy of the analytical method, the Vickers hardness of 0.46 percent carbon steel and 70/30 brass is analyzed, and the results compared with experimental results. The state of crack formation around the indentation in ceramics is investigated by considering the stress distribution around the indentation.

3.1 Analysis of the Vickers Hardness of 0.46 Percent C Steel. Figure 5 steel shows the stress-strain curves of 0.46 percent C steel and 70/30 brass in tensile tests. The true stress-logarithmic strain curves are used for the Vickers hardness analysis, and show that the yield stress of 0.46 percent C steel is 337 MPa.

The Hv specimen is cylindrical in shape with a diameter of 15 mm and height of 10 mm. The maximum load $P_{\max}$ is 490 N (50 kgf). Although the shape of the specimen for the analysis is different to that for the experiment, both specimen sizes are much larger than the dimension of indentation and the resulting plastic zone.

The preliminary calculations showed that the difference in boundary conditions at the support with regard to the plane ABC of Fig. 4(*a*) has little effect on the stress distribution except for the elements near the point B. Thus, it is expected

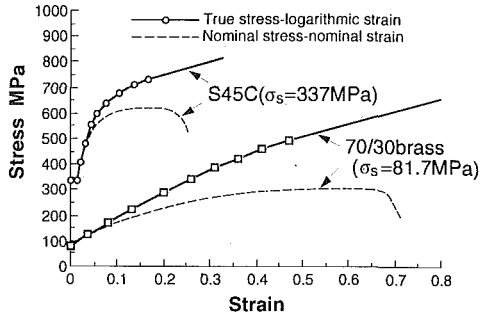

Fig. 5 Stress-strain curve of 0.46 percent C steel and 70/30 brass

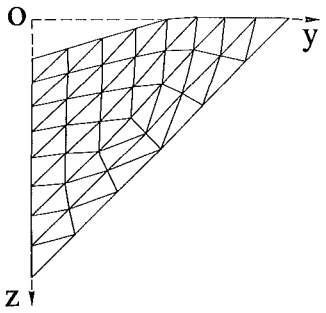

Fig. 6 Deformed shape of element near the origin (0.46 percent C steel, $P = P_{max}$)

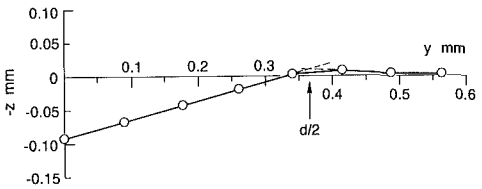

Fig. 7 Shape of diagonal of indentation after unloading (0.46 percent C steel)

that if the specimen size for the analysis is sufficiently larger than the extension of the plastic zone, the analysis should correlate well with the experimental results for the Vickers hardness. In this study, therefore, the displacement boundary condition $\Delta u = \Delta v = \Delta w = 0$ for the plane ABC of Fig. 4(*a*) is adopted.

Figure 6 shows the deformed shape of elements near the origin for $P = P_{max} = 490$ N (50 kgf). Figure 7 shows the shape of the indentation diagonal after unloading. The five nodal points nearest the origin are in contact with the indenter at $P = P_{max}$, and they are approximately in a straight line after unloading. The determination of the indentation size d in the analysis is in a sense somewhat arbitrary; there is no absolute definition of the indentation size in the analysis. In this study, the edge of the indentation was defined as shown in Fig. 7 by the intersection of two lines. The first is the line extended from the center of indentation and the second is the line extended from outside of the indentation. Thus, the Vickers hardness is calculated as follows.

$$Hv = \frac{2P_{max}}{d^2}\sin(\alpha/2) = \frac{2\times 50}{0.734^2}\times 0.9272 = 172 \text{ kgf/mm}^2 \quad (15)$$

To investigate the effect of mesh size on the accuracy of the results, several additional calculations using a fine mesh were performed. The results were almost identical to those already obtained. In the additional calculations, 13 nodal points were in contact with the indenter for 0.46 percent C steel. (In the original calculation, only five nodal points were in contact with the indenter.)

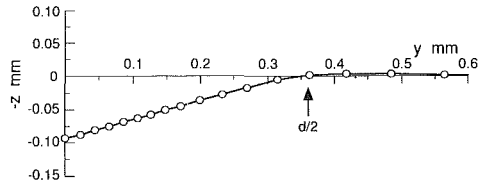

Fig. 8 Shape of diagonal of indentation after unloading by the analysis of fine mesh (0.46 percent C steel)

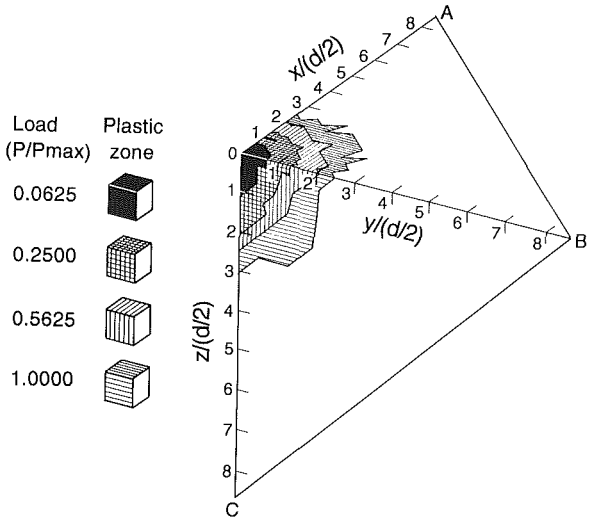

Fig. 9 Extension of plastic zone in 0.46 percent C steel specimen (*d*: diagonal of the indentation)

Table 1 Comparison of calculated results by conventional mesh and fine mesh

	(1/4 specimen)		(0.46%C steel)	
	Nodes	Elements	Hv	Depth of indentation
Original mesh	581	2376	172	0.0923mm
Fine mesh	1169	4968	176	0.0938mm

Figure 8 shows the shape of the indentation diagonal after unloading. The calculations are shown in Table 1. Thus, it may be concluded that the original mesh is sufficient for obtaining accurate results.

Figure 9 shows the extension of the plastic zone in the specimen at several loading steps. The elements which satisfy the Von Mises yield criterion within ±1 percent error are regarded as yielded elements. For the load $P = P_{max}$, the extension of the plastic zone on the specimen surface is 2.5 ~ 2.7 times the diagonal of indentation and the periphery of the plastic zone is almost circular in shape. The depth of the plastic zone is approximately 1.5 times the diagonal of the indentation and 12 times the indentation depth. These types of numerical results will enable one to understand the effect of specimen size and the existence of inhomogeneities near the point of measurement on empirically measured values of Hv. These problems must be addressed in more detail in future research.

Figure 10 shows the stress distribution in the vicinity of the y-axis for $P = P_{max}$. At the center of the contact surface, σ_z is approximately twice the value of σ_y. This result closely resem-

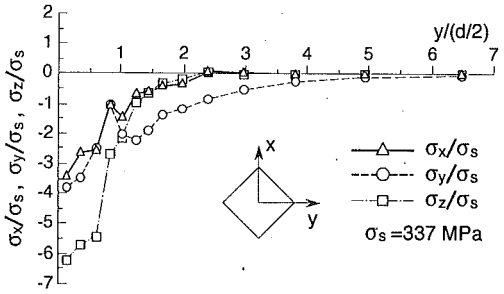

Fig. 10 Stress distribution in the vicinity of y-axis (0.46 percent C steel, $P = P_{max}$)

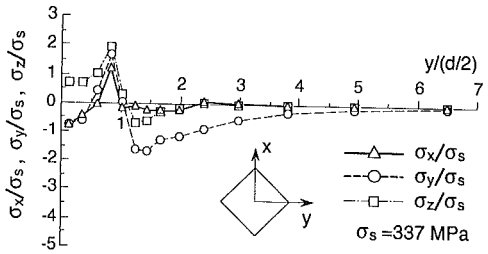

Fig. 11 Residual stress distribution in the vicinity of y-axis (0.46 percent C steel)

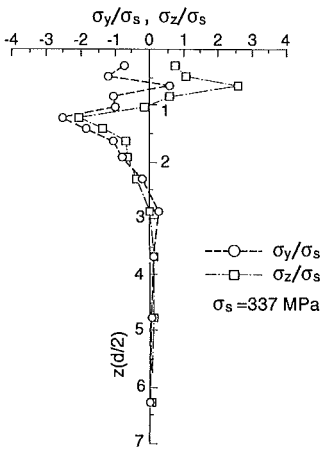

Fig. 12 Residual stress distribution in the vicinity of z-axis (0.46 percent C steel)

bles the numerical results of Brinell hardness (Murakami and Yuan, 1990, 1992). However, the maximum values of the three stresses σ_x, σ_y, and σ_z occur at the center of indentation. It should be noted that up to the point of unloading, there are no tensile stresses in the vicinity of the indenter. This is of critical importance regarding the question of whether indentation-induced cracking in ceramics initiates during loading or unloading. (This result was obtained using the mesh shown in Fig. 4.)

Figures 11 and 12 illustrate the distribution of residual stresses in the vicinity of y and z-axis, respectively, after unloading. The residual stresses σ_x and σ_y near the origin are compressive and they become tensile along the diagonal near the indentation edge (see Fig. 11). If these tensile stresses are the cause of crack initiation in ceramics, the crack should be formed during unloading. This is an important condition which must be taken into consideration when the stress intensity factor K of an indentation-induced crack is analyzed.

The comparatively large stresses σ_z in the vicinity of the indentation can be explained by considering the following two points. First, the values of σ_z are not the values at the actual free surface but average values of the elements near the surface.

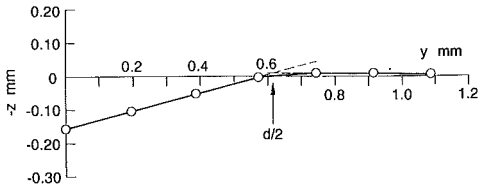

Fig. 13 Shape of diagonal of indentation after unloading (70/30 brass)

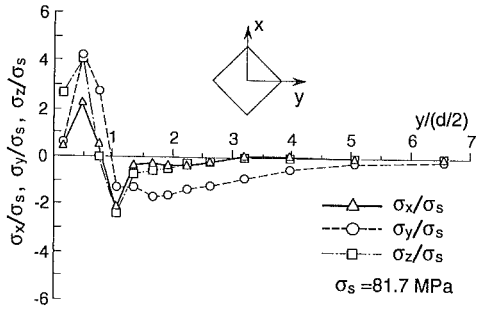

Fig. 14 Residual stress distribution in the vicinity of y-axis (70/30 brass)

Secondly, the indentation surface is inclined, thus leading to higher values in the z-direction. The tensile residual stresses σ_z in the vicinity of the z-axis in Fig. 12 are also important in relation to lateral cracks produced by the Vickers indentation test observed in glasses and other ceramics (Marshall and Lawn, 1979; Antis, Chantikal, Lawn, and Marshall, 1981).

3.2 Analysis of the Vickers Hardness of 70/30 Brass. Figure 5 shows the stress-strain curve of 70/30 brass in a tensile test and the true stress-logarithmic strain curve used for the Vickers hardness analysis. The yield stress of 70/30 brass is 81.7 MPa. The applied maximum load P_{max} in the Vickers hardness test and analysis is 490 N (50 kgf). The finite element method mesh pattern is the same as that for 0.46 percent C steel, though the size is approximately twice that for 0.46 percent C steel since the extension of the plastic zone is much greater.

Figure 13 shows the shape of indentation diagonal after unloading. According to Fig. 13, the diagonal of indentation is 1.236 mm and accordingly the Vickers hardness Hv is 60.7 kgf/mm^2.

The extension shape of the plastic zone in the specimen at several loading steps is almost identical to that of 0.46 percent C steel (Fig. 9). The stress distribution in the vicinity of the y-axis for $P = P_{max}$ is also almost identical to that of 0.46 percent C steel (Fig. 10). Figures 14 and 15 illustrate the distribution of residual stresses in the vicinity of the y and z-axes, respectively, after unloading. The residual stresses σ_x and σ_y near the y-axis in the indentation are both tensile.

3.3 Effect of Hardening Rules. The above results are based on isotropic hardening. However, phenomena such as the Bauschinger effect in engineering materials make the results inconsistent with the isotropic hardening rule. Furthermore, the application of alternative hardening rules yields a different set of analytical results.

To investigate the effect of different hardening rules, the Vickers hardness of elastic-linear-hardening materials was analyzed based firstly on the isotropic hardening rule and secondly on the kinematic hardening rule. The yield stress σ_y in the basic stress strain curve is 392 MPa (40 kfg/mm^2) and the plastic strain-hardening modulus H' ($= d\sigma/d\epsilon_p$) is 4900 MPa (500 kgf/mm^2). (Prager's rule (Prager, 1955) was used for the kinematic hardening rule.)

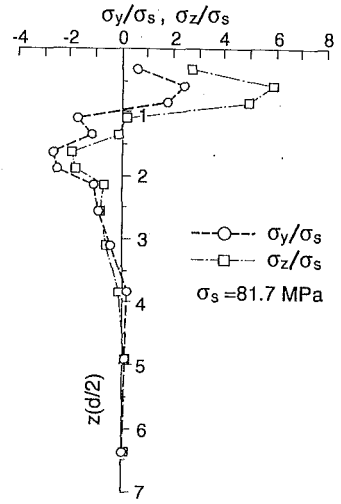

Fig. 15 Residual stress distribution in the vicinity of z-axis (70/30 brass)

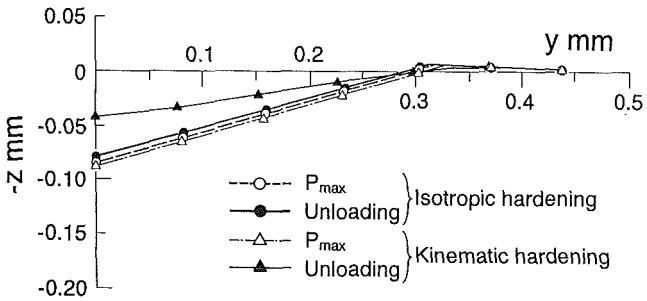

Fig. 16 Comparison of the numerical results based on the isotropic hardening rule and the kinematic hardening rule ($\sigma_s = 392$ MPa, $H' = d\sigma/d\epsilon_p = 4900$ MPa)

Figure 16 shows the analytical results for two hardening results. The indenter displacements for $P = P_{max}$ in the kinematic hardening rule ($\triangle$) are only 3.7 percent higher than that in the isotropic hardening ($\circ$). However, while the recovery of the maximum indentation displacement from $P = P_{max}$ to $P = 0$ is 6.5 percent for the isotropic hardening rule, that for the kinematic hardening rule exceeds 50 percent. These results clearly indicate the remarkable effect that the hardening rules have upon indentation displacement. The experimentally measured depth from the edge of the indentation to the base is 104 μm for 0.46 percent carbon steel and 168 μm for 70/30 brass. The calculated results based on the isotropic hardening rule (100 μm for 0.46 percent carbon steel and 168 μm for 70/30 brass) correlate well with the experimental results. However, it should be noted that the hardening rule has little effect on the analytical values of the Vickers hardness (i.e., less than two percent in the isotropic hardening rule and less than six percent in the kinematic hardening rule).

3.4 Comparison of Numerical Results With Experimental Results. Table 2 compares the numerical and experimental results for 0.46 percent carbon steel and 70/30 brass. For both materials good correlation exists between the numerical and experimental results.

3.5 Tensile Residual Stresses Induced by Indentation and Initiation of Indentation Cracks in Ceramics. As shown in Fig. 11 and Fig. 14, after unloading there is large tensile residual stress in the vicinity of the indentation for 0.46 percent carbon steel and 70/30 brass. The locations of the maximum tensile stress peaks are dependent upon material type and differ slightly for 0.46 percent carbon steel and 70/30 brass. Since exact

Table 2 Comparison of the numerical results with experimental ones of 0.46 percent C steel and 70/30 brass

		Load P_{max}	Diagonal of indentation d (mm)	Vickers hardness Hv
0.46%C steel	Experiment	490N(50kgf)	0.737	171
	Calculation	490N(50kgf)	0.734	172
70/30brass	Experiment	490N(50kgf)	1.229	61.4
	Calculation	490N(50kgf)	1.236	60.7

stress-strain curves (i.e., constitutive equations of ceramics) are not known, it is difficult to determine the location and value of the maximum tensile stress. However, the elastic-plastic response to indentation for metals may be qualitatively applied to ceramics.

The indentation technique for measuring fracture toughness K_{Ic} of brittle materials such as ceramics has been studied by many investigators (Chiang, Marshall, and Evans, 1982; Tanaka, 1984; Lawn and Marshall, 1978; Lankford and Davidson, 1979; Niihara, 1983; Shetty, Wright, Mincer, and Clauer, 1985; Keer, Farris, and Lee, 1986; Li, Ghosh, Kobayashi, and Bradt, 1989; Yingzhi and Hills, 1990; Marshall and Lawn, 1979; Antis, Chantikal, Lawn, and Marshall, 1981). However, since the exact stress state around the indentation with cracks is not known, many equations for the determination of K_{Ic} were proposed by combining dimensional analysis for the indentation crack and K_{Ic} values measured using the standard fracture mechanics techniques. The K_{Ic} equations based on the Lawn, Evans, and Marshall model (Lawn, Evans, and Marshall, 1980) and the internal inclusion model (Tanaka, Kitahara, Ichinose, and Iimura, 1984) were also proposed. In addition, there are reports (Keer, Farris, and Lee, 1986; and Li, Ghosh, Kobayashi, and Bradt, 1989) of an elastic numerical analysis in which the indentation load is replaced by a concentrated point force. Nevertheless, it should be noted that most of these models assume that indentation cracks are formed at the loading process rather than the unloading process (Lankford, 1979). However, some reports (Marshall and Lawn, 1979; Antis, Chantikal, Lawn, and Marshall, 1981) indicate that the behavior of the materials during the unloading process cannot be ignored when considering crack formation.

The question as to whether it is the loading or unloading process which has the more critical effect on crack formation was investigated experimentally. The plastic replicas taken from the vicinity of indentation at $P = P_{max}$ and after unloading ($P = 0$) were compared.[1] Figures 17(a) and (b) show the photographs of two plastic replicas at $P = P_{max}$ and after unloading. These indicate that the crack initiated at the unloading process. Therefore, it may be concluded that the residual tensile stress during the unloading process has an important effect on the behavior of crack initiation and also upon its subsequent arrest. However, the authors have recently observed crack initiation during the loading process in some other ceramics. Thus, the phenomena during micro-indentation and the response of ceramics would appear to be very complicated.

Since material properties influence the distribution of residual stresses, it seems possible that the equations proposed by many investigators for the determination of K_{Ic} based on the size of the crack formed around the indentation and the max-

[1] In the soft state (immediately after being dipped in solution) the plastic replica is spread around the diamond indenter at $P = P_{max}$. Once the plastic replica has rehardened, the diamond indenter is removed and the specimen is unloaded. Thus, it is possible to observe the behavior of the specimen at maximum load, though the center of the replica is vacant (as shown in Fig. 17(a)). A second plastic replica is then spread over the indentation, once the material has been unloaded. In this way, it is possible to observe the state of the crack formation during the process of unloading.

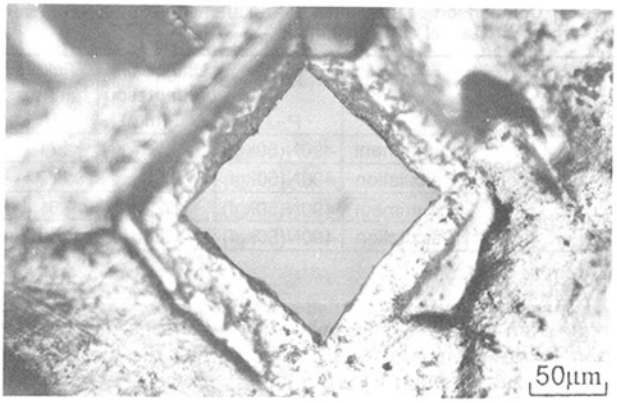

Fig. 17(*a*) Photograph of plastic replica of $P = P_{max}$ (20 kgf)

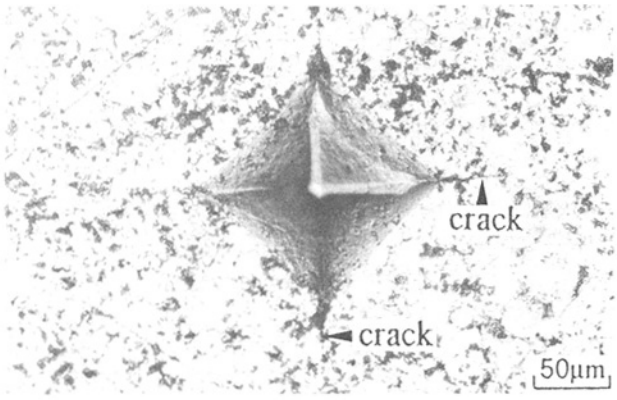

Fig. 17(*b*) Photograph of plastic replica after unloading

Fig. 17 State of crack formation of Al_2O_3-TiC under the Vickers hardness test

imum load could be applicable to just one specific material. Thus, for the determination of K_{Ic} of ceramics by the so-called "micro-indentation method," it might be necessary in some cases to closely study the position and timing of crack formation.

4 Conclusion

(1) A particular formulation of the three-dimensional finite element method for the Vickers hardness test is established.

(2) The Vickers hardness of 0.46 percent carbon steel and 70/30 brass are analyzed by the proposed method. The calculated values show good correlation with the experimentally measured hardness.

(3) At the maximum load of indentation process there is no tensile stress in the vicinity of the indenter. However, after removal of the load, large tensile residual stresses are induced at the diagonal edge beneath the indentation. These results imply that crack initiation in ceramics during the indentation test may occur mainly during the unloading process. Therefore, the validity of the so-called micro-indentation method for the determination of K_{Ic} of ceramics must be carefully reconsidered.

Acknowledgments

The authors wish to express their thanks to Prof. T. N. Farris, Purdue University, for the useful discussion on this paper and for his kindness in revising the English manuscript.

References

Anstis, G. R., Chantikul, P., Lawn, B. R., and Marshall, D. B., 1981, "A Critical Evaluation of Indentation Techniques for Measuring Fracture Toughness: I. Direct Crack Measurements," *J. Am. Ceram. Soc.*, Vol. 64, pp. 533–538.

Chiang, S. S., Marshall, D. B., and Evans, A. G., 1982, "The Response of Solids to Elastic/Plastic Indentation. I. Stresses and Residual Stresses," *J. Appl. Phys.*, Vol. 53, pp. 298–311.

Keer, L. M., Farris, T. N., and Lee, J. C., 1986, "Knoop and Vickers Indentation in Ceramics Analyzed as a Three-Dimensional Fracture," *J. Am. Ceram. Soc.*, Vol. 69, No. 5, pp. 392–396.

Lankford, J., and Davidson, D. L., 1979, "The Crack Initiation Threshold in Ceramic Materials Subject to Elastic/Plastic Indentation," *J. Materials Sci.*, Vol. 14, pp. 1662–1668.

Lawn, B. R., Evans, A. G., and Marshall, D. B., 1980, "Elastic/Plastic Indentation Damage in Ceramics: The Median/Radial Crack System," *J. Am. Ceram. Soc.*, Vol. 63, pp. 574–581.

Lawn, B. R., and Marshall, D. B., 1978, *Fracture Mechanics of Ceramics*, Vol. 3, edited by R. C. Bradt, D. P. H. Hasselman, and F. F. Lange, Plenum, New York, pp. 205–209.

Li, Z., Ghosh, A., Kobayashi, A. S., and Bradt, R. C., 1989, "Indentation Fracture Toughness of Sintered Silicon Carbide in the Palmqvist Crack Regime," *J. Am. Ceram. Soc.*, Vol. 69, pp. 904–911.

Marshall, D. B., and Lawn, B. R., 1979, "Residual Stress Effects in Sharp Contact Cracking, Part 1. Indentation Fracture Mechanics," *Journal of Materials Science*, Vol. 14, pp. 2001–2012.

Mindlin, R. D., 1936, "Force at a Point in the Interior of a Semi-Infinite Solids," *Physics*, Vol. 7, pp. 195–202.

Mura, T., Yamashita, N., Mishima, T., and Hirose, Y., 1989, "A Dislocation Model for Hardness Indentation Problems—I," *Int. J. Engng. Sci.*, Vol. 27, pp. 1–9.

Murakami, Y., and Yuan, L. P., 1990, "Analysis of Brinell Hardness by the Finite Element Method (Particular Formulation and Comparison with Experimental Results)," submitted to *Int. J. Solids & Structures*.

Murakami, Y., and Yuan, L. P., 1992, "Finite Element Method (FEM) Analysis of Elastic-Linear-Hardening Materials and Comparison with Measurement on Commercial Materials," *ASTM Journal of Testing and Evaluation*, Vol. 20, pp. 15–24.

Niihara, K., 1983, "A Fracture Mechanics Analysis of Indentation-induced Palmqvist Crack in Ceramics," *J. Materials Sci. Letters*, Vol. 2, pp. 221–223.

Perrott, C. M., 1977, "Elastic-Plastic Indentation: Hardness and Fracture," *Wear*, Vol. 45, pp. 293–309.

Ponton, C. B., and Rawlings, R. D., 1989, "Dependence of the Vickers Indentation Fracture Toughness on the Surface Crack Length," *British Ceram. Trans. J.*, Vol. 88, pp. 83–90.

Prager, W., 1955, "Theory of Plasticity: A Survey of Recent Achievement," *Proc. Inst. Mech. Eng.*, Vol. 169, pp. 41–57.

Shetty, D. K., Wright, I. G., Mincer, P. N., and Clauer, A. H., 1985, "Indentation Fracture of WC-Co Cermets," *J. Materials Sci.*, Vol. 20, pp. 1873–1882.

Tabor, D., 1951, *The Hardness of Metals*, Oxford University Press, London.

Tanaka, K., 1984, "Evaluation of Elastic/Plastic Indentation Stress to Determine Fracture Toughness," *Trans. Japan Inst. Metals*, Vol. 48, pp. 1157–1162 (in Japanese).

Tanaka, K., Kitahara, Y., Ichinose, Y., and Iimura, T., 1984, "Fracture Analysis of Single Crystal Manganese Zinc Ferrites Using Indentation Flaws," *Acta Metall.*, Vol. 32, pp. 1719–1729.

Westbrook, J. H., and Conrad, H., 1973, *The Science of Hardness Testing and Its Research Applications*, American Society for Metals, Metals Park, Ohio.

Yingzhi, L., and Hills, D. A., 1990, "The Analysis of Three-Dimensional Cracks Generated by Sharp Indentation," *J. Mech. Phys. Solids*, Vol. 38, pp. 255–272.

Yoshino, T., and Yamada, M., 1984, "FEM Analysis of Elastic Indentation Stress of Pyramidal Indenter," *Tran. Japan Soc. Mech. Engrs.*, Vol. 50, pp. 1628–1636 (in Japanese).

Yoshizawa, T., 1967, *The Hardness Testing and Its Application*, Shokabo Press, Tokyo (in Japanese).

Zienkiewicz, O. C., 1971, *The Finite Element Method in Engineering Science*, McGraw-Hill, London.